

Weak hierarchy of turbulent dynamics in a semiconductor experiment

J. Parisi, J. Peinke, and R.P. Huebener

Physikalisches Institut, Lehrstuhl Experimentalphysik 11, Universität Tübingen, Morgenstelle 14, D - 7400 Tübingen, Fed. Rep. Germany

R. Stoop

Physik-Institut, Universität Zürich, Schönberggasse 9, CH-8001 Zürich, Switzerland

M. Duong-van

Physics Department, Lawrence Livermore National Laboratory, University of California, P.O. Box 808, Livermore, CA 94550, USA

Received 7 July 1989

Abstract Nonlinear current transport behavior during low-temperature impact ionization breakdown of extrinsic germanium comprises the self-sustained development of both filamentary spatial and oscillatory temporal dissipative structures in the formerly homogeneous semiconductor. We study the cooperative spatio-temporal breakdown phenomena via both probabilistic and dynamical characterization methods. Agreement between the results obtained from the different numerical concepts gives a self-consistent picture of the physical situation investigated. As a consequence, the affirmed chaotic hierarchy of generalized horseshoe-type strange attractors may be ascribed to weak nonlinear coupling between competing localized oscillation centers intrinsic to the present semiconductor system.

1. Introduction

Certain systems, with dynamics governed by partial differential equations, exhibit complexity that is no worse than that of a few coupled nonlinear ordinary differential equations. These systems have been studied extensively as part

Paper presented at the 17th IUPAP International Conference on Thermodynamics and Statistical Mechanics, Rio de Janeiro, 31 July - 04 August 1989.

functions. Verification of the Kaplan-Yorke conjecture and the **Newhouse-Ruelle-Takens** theorem fits well into the model of **spatially** localized and weakly coupled oscillatory subsystems inherent to the global multicomponent semiconductor **system** considered.

2. Experimental

Our experiments were performed on single-crystalline **p-type** germanium material, having the dimensions of about $0.25 \times 2 \times 5 \text{ mm}^3$ and an impurity doping concentration of about $3 \times 10^{14} \text{ cm}^{-3}$ of indium, aluminum, and gallium acceptors (corresponding to shallow acceptor levels in the range of 10 meV above the valence band edge). The compensation ratio was definitely smaller than 5×10^{-2} . The specific resistivity at room temperature amounted to about $10 \text{ } \Omega\text{cm}$. During sample preparation, the extrinsic germanium crystal was successively polished (with diamond paste) and etched (with **CP4**), in order to obtain an ideal surface structure. Then properly arranged ohmic aluminum contacts were evaporated upon one of the two largest crystal surfaces. For alloying the contact with the bulk material, the sample was heated above the eutectic point of the system.

To provide the outer ohmic contacts with an electric field, a d.c. bias voltage (V_0) was applied to the series combination of the sample and the load resistor (R_L). A d.c. magnetic field (**B**) perpendicular to the broad sample surfaces could also be applied by a superconducting solenoid surrounding the semiconductor sample. The resulting electric current **I** was found from the voltage drop at the load resistor. The voltage **V** was measured between the two outer contacts of the sample. Two additional inner probe contacts (of about 0.2 mm diameter) that are placed equidistantly in between served for monitoring independently the lateral partial voltages V_i ($i = 1, 2, 3$) along the sample. During the experiments, the semiconductor sample was always kept at liquid-helium temperature ($T = 4.2\text{K}$) and carefully protected against external electromagnetic irradiation (visible, far infrared). Further details on the experimental techniques can be found elsewhere³.

3. Physics

Analogous to the corresponding processes of structure formation in gaseous plasma discharges, impact ionization of the shallow impurity acceptors can be achieved in the bulk of the homogeneously doped semiconductor at low temperatures. In the temperature range of liquid helium, most of the charge carriers are frozen out at the impurities. Since the ionization energy is only about 10 meV and electron-phonon scattering is strongly reduced, avalanche breakdown already takes place at electric fields of a few V/cm and persists until nearly all impurities are ionized. The transport mechanism involved in the nondestructive breakdown phenomenon can be attributed to impact ionization of the impurities by mobile charge carriers heated via the applied electric field⁴.

The underlying nonequilibrium phase transition from a low conducting state to a high conducting state is directly reflected in strongly nonlinear regions of negative differential resistivity in the microscopic current-density versus electric-field characteristic⁵. Accordingly, the autocatalytic process of impurity impact ionization also leads to a strongly nonlinear curvature of the macroscopic (measured) current-voltage characteristic (with sometimes S-shaped negative differential resistance⁶), the nonlinearity occurring just beyond the voltage corresponding to the critical electric field where the current increases by many orders of magnitude (typically, from a few nA in the pre-breakdown up to a few mA in the post-breakdown region⁴).

Under slight variation of distinct control parameters (electric field, magnetic field, and temperature in the range of some 10^{-6} V/cm , 10^{-1} G , and 10^{-3} K , respectively) the resulting electric current flow displays a wide variety of spatio-temporal nonlinear transport behavior. As described previously, low-temperature avalanche breakdown develops the self-sustained formation of filamentary current flow patterns associated with the appearance of spontaneous current and voltage oscillations². Note that these state variables show - superimposed upon the d.c. current and voltage signals of typically a few mA and some hundred mV ,

respectively - temporal oscillations with a relative amplitude of about 10^{-3} in the frequency range 0.1 - 10 *kHz*.

4. Results and Discussion

The complex spatial behavior of our semiconductor system can be globally visualized by means of low-temperature scanning electron microscopy⁷. Fig. 1 shows a two-dimensional image of a typical current filament pattern developing in the nonlinear post-breakdown regime of the current-voltage characteristic (parameters $V_0 = 2.0V$, $R_L = 1V$, $B = 1G$). As reported elsewhere⁸ in detail, nucleation of additional filaments is often accompanied by abrupt changes between different stable filament configurations via noisy current instabilities. Moreover, the simultaneous spatial identification of oscillatory current flow dynamics provides a powerful tool for gaining deeper insight into the mutual interplay between spatial and temporal current structures. In the spirit of chaotic hierarchy¹, turbulent dynamics may thus be ascribed to nonlinear coupling between competing localized oscillation centers intrinsic to our semiconductor system. So far, we have demonstrated experimentally the existence of spatially separated oscillatory subsystems¹⁰ as well as their long-range interaction¹¹.

In this experiment, we concentrate on the quantitative characterization of the cooperative temporal behavior induced by the avalanche breakdown kinetics of our multicomponent semiconductor system. For evaluating the hierarchical tree of the chaotic order proposed, we apply distinct numerical analysis procedures embracing both probabilistic and dynamical concepts. As a first step, we examine two characteristic data files of spontaneous voltage oscillations $V_2(t, ; n = 1..80000)$, obtained for the different working conditions $B = 31.5G$ (file A) and $B = 46.5G$ (file B) at constant parameters $V_0 = 2.145V$, $R_L = 100V$, and $T = 4.2K$. These cases were selected taking into account the different structural shape of the phase portraits shown in fig. 2. The two-dimensional representation $V_2(t,)$ vs $V_2(t, + \tau)$ of the trajectories in phase space is constructed by using an appropriate sampling rate of 100 *kHz* and a delay time of 50 μs (embedding theorem¹²). As already pointed out in an earlier conjecture¹³, the phase portrait of fig. 2(a) is suggestive

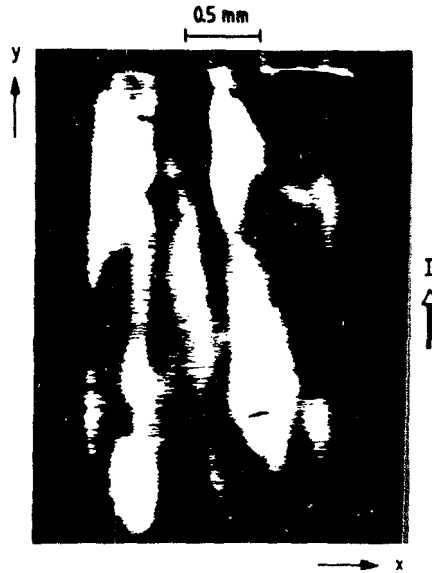


Fig.1 - Brightness-modulated image of the **filamentary** current **flow** in the homogeneous **bulk** semiconductor during avalanche breakdown obtained by low-temperature scanning electron microscopy. The **spatially resolved imaging** is **accomplished** by scanning the specimen **surface** with an electron beam and by recording the beam-induced current change in the **voltage-biased** specimen as a function of the beam coordinate (x,y) . The dark regions correspond to the filament **channels** extending **along** the y -direction. For **details**, **ref.8**.

of a strange attractor having a dimension larger than two. The attractor can be visualized as a curled band partly folded over, embedded in three-dimensional space. This impression was especially striking when the bias voltage was slightly varied in the 0.1 percent range, resulting in a different projection of the same object. Upon increasing the magnetic field, the curled band structure (fig. 2(a)) gradually changed into a spherical tangle (fig.2(b)) with increasing attractor dimensionality, apparently representing a higher state of chaos. The trajectories occupy the interior of a nearly spherical portion of the projected phase space. This picture did not change under small variations of the control parameters (cf. fig. 3 of ref.13).

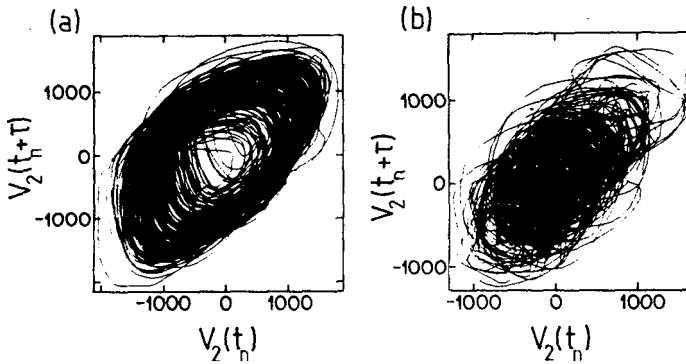


Fig.2 - Phase plots of different chaotic attractors generated from parts of the data files A (a) and B (b). Note that 1000 arbitrary units correspond to about 5 mV signal amplitude. The characteristic frequencies are below 5 kHz.

In the following, we briefly report the quantification of the present experimental situation with the help of generalized fractal dimensions, entropies, Lyapunov exponents, and the corresponding scaling functions. The fundamentals of the characterization methods applied are described elsewhere¹⁴ in detail. First, the generalized fractal dimensions $D(q)$ and the generalized entropies $K(q)$ were calculated with the nearest-neighbor algorithm proposed by Badii and Politi¹⁵. Taking into account the scaling behavior of the next-neighbor distance at a generic point with the number of trial points, the dimensions and entropies could be extracted directly from the slope and the shift of the successive log-log plots, respectively, obtained with increasing dimension of the embedding phase space¹⁶. The results computed for the two characteristic data files are listed in table I. Here we have used embeddings of dimension from 20 to 26 (cf. fig. 5 of ref. 14). We conclude that the states A and B manifest different strange attractors, the chaotic behavior of the second one reflecting a considerably higher degree of freedom. The closeness of $D(0)$ and $D(1)$ as well as $K(0)$ and $K(1)$ indicates an almost self-similar structure for both chaotic attractors, not yet being adequate to confirm multifractal behavior of the system. In order to yield a more complete characterization, we

looked at the spectra of invariant static scaling indices $f(\alpha)$ describing the global distribution of singularities on a fractal measure¹⁷. Their graphs are given in fig. 3 for the two data files considered. It is now clearly seen that both chaotic attractors display multifractal structures, the extension and the form of which are changed drastically between the two working conditions. Moreover, the numerical values of the generalized fractal dimensions are fairly well reproduced by the corresponding scaling functions.

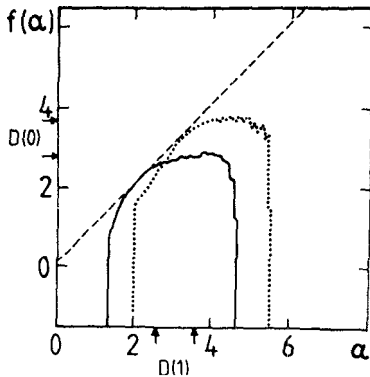


Fig.3 - Static scaling functions of different chaotic attractors calculated from the data files A (solid curve) and B (dotted curve). Note that the values of $D(0)$ and $D(1)$ indicated by arrows on the ordinate and the abscissa correspond to the maximum and the tangential point with the diagonal of the spectrum of dimensions, respectively.

Finally, we have evaluated the generalized Lyapunov exponents λ_i together with the corresponding spectra of invariant dynamical scaling indices $\Phi(\Lambda)$ using the algorithm developed by Stoop and Meier¹⁸. The Lyapunov characteristic exponents were estimated from the linearized dynamics constructed by a least-squares fit, based on a modified and improved version of the proposals put forward by Eckmann et al¹⁹ and Sano et al^{16,20}. As summarized in table 1, we detected three (four) relevant exponents from data file A (B) for embeddings of dimension from 7 to 10 (8 to 11). In accordance with the gradually increasing dimensionality, the two chaotic states are further discriminated by a different number of positive Lyapunov exponents, determining mutually independent directions of stretching and folding-over of nearby trajectories in phase space and, thus, reflecting the order of chaos¹⁸⁻²¹. Adopting the terminology introduced by Rössler^{1,22}, the

Weak hierarchy of turbulent dynamics in a...

first state is called "ordinary chaotic" (three-variable chaos defined by one positive exponent), the higher-order analogue of the second state "hyperchaotic" (four-variable chaos defined by two positive exponents). The global spectral characterization of these chaotic dynamics can be deduced from the scaling functions for the generalized Lyapunov exponents²³. Their graphs in fig. 4 show the different dynamical complexity of the attractors. The spreading and the shifted position of the $\Phi(\Lambda)$ spectra are qualitatively seen in $f(\alpha)$. Again, the numerical values of the generalized entropies can be reproduced by the corresponding dynamical scaling functions¹⁴.

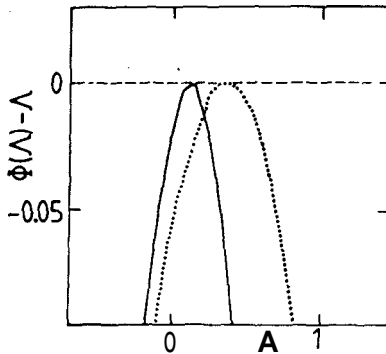


Fig.4 - Dynamical scaling functions of different chaotic attractors calculated from the data files A (solid curve) and B (dotted curve).

One conjecture that unifies probabilistic and dynamical properties of an attracting set is the Kaplan-Yorke relationship²⁴. Therefore, we derived from the Lyapunov spectrum the corresponding dimension

$$D = j + \sum_{i=1}^j \lambda_i / |\lambda_{j+1}| ,$$

where j is defined by the condition that

$$\sum_{i=1}^j \lambda_i > 0 \quad \text{and} \quad \sum_{i=1}^{j+1} \lambda_i < 0 .$$

The results obtained for the two chaotic attractors are given in table 1. Comparison between the Lyapunov dimension D and the information dimension $D(\mathbf{1})$ calculated independently shows satisfactory agreement within experimental accuracy

of one standard deviation. A further conjecture predicts that the Kolmogorov-Sinai entropy $K(1)$ corresponds to the lower bound of the sum of all positive Lyapunov exponents^{19,25}. The apparent closeness of these quantities in our experiment (in contrast to other dynamical systems²⁶) may indicate the manifestation of near-quasiperiodic strange attractors that are governed by horseshoe-like diffeomorphisms (Newhouse-Ruelle-Takens theorem^{1,25,27}). We suspect that the chaotic hierarchy inherent to the present semiconductor system is generated by *weak* nonlinear coupling of spatially localized oscillatory **subsystems**. Indeed, we have found that the evaluation of dimensions, entropies, Lyapunov exponents, and corresponding scaling functions for different local **voltage drops** V_i along the sample yields nearly identical **results** - in accordance to earlier **conjectures**^{10,13}.

Table 1 - Comparison of characteristic quantities for different chaotic **states**. The values of the entropies and the Lyapunov exponents are in units of the sampling rate.

	File A	File B
Fractal Dimensions	$D(O) = 2.6 \pm 0.1$	$D(O) = 3.6 \pm 0.1$
	$D(1) = 2.5 \pm 0.1$	$D(1) = 3.5 \pm 0.1$
Entropies	$K(0) = 0.09 \pm 0.01$	$K(0) = 0.15 \pm 0.01$
	$K(1) = 0.09 \pm 0.01$	$K(1) = 0.15 \pm 0.01$
Lyapunov Exponents	$\lambda_1 = 0.095 \pm 0.005$	$\lambda_1 = 0.159 \pm 0.005$
	$\lambda_2 = 0.003 \pm 0.005$	$\lambda_2 = 0.076 \pm 0.005$
	$\lambda_3 = -0.72 \pm 0.02$	$\lambda_3 = -0.021 \pm 0.005$
		$\lambda_4 = -0.77 \pm 0.03$
Lyapunov Dimensions	$D = 2.1 \pm 0.2$	$D = 3.3 \pm 0.1$

5. Conclusions

An exemplary semiconductor system is shown to undergo different degrees of chaotic behavior. With the help of distinct numerical analysis procedures,

a self-consistent picture of the physical situation investigated is obtained. This picture fits well into the model of a multicomponent reaction-diffusion system, capable of generating a weak chaotic hierarchy of near-quasiperiodic strange attractors. From preliminary studies of coupled map lattices, one might speculate that a universal scaling law should be observed on the ladder towards higher chaos, analogous to that discovered by Feigenbaum and Grossmann for the successive, ever closer-spaced appearance of higher and higher periodic solutions ending in chaos. Moreover, it appears possible that some of the phase transitions in physics known to obey a scaling law in space have properties in common with the present deterministic spatio-temporal phenomenon. A first hint is probably given by a phase-transition-like behavior drawn from the probabilistic and dynamical scaling functions of the hyperchaotic state²⁸.

The authors would like to thank Otto E. Rössler for exchange of ideas. This work has been supported financially by the Volkswagen-Stiftung and the Swiss National Foundation. M.D. benefitted from a three-month visit at the University of Tiibingen, which was financed by the Deutsche Forschungsgemeinschaft.

References

1. O.E. Rössler, *Z. Naturforsch.* 38 a, 788 (1983).
2. For an overview see: R.P. Huebener, K.M. Mayer, J. Parisi, J. Peinke, and B. Röhrich, *Nucl. Phys. B (Proc. Suppl.)* 2, 3 (1987); J. Peinke, J. Parisi, B. Röhrich, K.M. Mayer, U. Rau, and R.P. Huebener, *Solid State Electron.* 31, 817 (1988), and references therein.
3. J. Peinke, J. Parisi, B. Röhrich, K. M. Mayer, U. Rau, W. Clauss, R.P. Huebener, G. Jungwirt, and W. Prettl, *Appl. Phys. A* 48, 155 (1989).
4. J. Parisi, U. Rau, J. Peinke, and K.M. Mayer, *Z. Phys. B - Condensed Matter* 72, 225 (1988).
5. E. Schöll, *Nonequilibrium Phase Transitions in Semiconductors* (Springer, Berlin, 1987).

6. J. Peinke, D.B. Schmid, B. Röhricht, and J. Parisi, *Z. Phys. B - Condensed Matter* **66**, 65 (1987).
7. R.P. Huebener, in *Advances in Electronics and Electron Physics*, vol. 70, ed. P.W. Hawkes (Academic Press, New York, 1988) p.1.
8. K.M. Mayer, R. Gross, J. Parisi, J. Peinke, and R.P. Huebener, *Solid State Commun.* **63**, 55 (1987); K.M. Mayer, J. Peinke, B. Rohricht, J. Parisi, and R.P. Huebener, *Physica Scripta T* **19**, 505 (1987).
9. K.M. Mayer, J. Parisi, J. Peinke, and R.P. Huebener, *Physica* **32 D**, 306 (1988).
10. J. Peinke, J. Parisi, B. Röhricht, B. Wessely, and K. M. Mayer, *Z. Naturforsch.* **42 a**, 841 (1987).
11. B. Rohricht, J. Parisi, J. Peinke, and R.P. Huebener, *Z. Phys. B - Condensed Matter* **66**, 515 (1987).
12. N.H. Packard, J.P. Crutchfield, J.D. Farmer, and R.S. Shaw, *Phys. Rev. Lett.* **45**, 712 (1980); F. Takens, in *Lecture Notes in Mathematics*, vol. 898, eds. D.A. Rand and L.-S. Young (Springer, Berlin, 1981) p.366.
13. J. Peinke, B. Rohricht, A. Muhlbach, J. Parisi, Ch. Nöldeke, R.P. Huebener, and O.E. Rössler, *Z. Naturforsch.* **40 a**, 562 (1985).
14. R. Stoop, J. Peinke, J. Parisi, B. Rohricht, and R. P. Huebener, *Physica* **35 D**, 425 (1989).
15. R. Badii and A. Politi, *J. Stat. Phys.* **40**, 725 (1985).
16. S. Sato, M. Sano, and Y. Sawada, *Prog. Theor. Phys.* **77**, 1 (1987).
17. T.C. Halsey, M.H. Jensen, L.P. Kadanoff, I. Procaccia, and B.I. Shraiman, *Phys. Rev. A* **33**, 1141 (1986).
18. R. Stoop and P.F. Meier, *J. Opt. Soc. Am. B* **5**, 1037 (1988).
19. J.-P. Eckmann and D. Ruelle, *Rev. Mod. Phys.* **57**, 617 (1985); J.-P. Eckmann, S. Oliffson Kamphorst, D. Ruelle, and S. Ciliberto, *Phys. Rev. A* **34**, 4971 (1986).
20. M. Sano and Y. Sawada, *Phys. Rev. Lett.* **55**, 1082 (1985).

21. V.I. Oseledec, Trans. Moscow Math. Soc. 19, 197 (1968); G. Benettin, L. Galgani, and J.M. Strelcyn, Phys. Rev. A 14, 2338 (1976); A. Wolf, J.B. Swift, H.L. Swinney, and J.A. Vastano, Physica 16 D, 285 (1985).
22. O.E. Rössler, Phys. Lett. 71 A, 155 (1979); O.E. Rössler, Lect. Appl. Math. 17, 141 (1979).
23. H. Fujisaka, Prog. Theor. Phys. 70, 1264 (1983); P. Grassberger and I. Procaccia, Physica 13 D, 34 (1984); J.-P. Eckmann and I. Procaccia, Phys. Rev. A 34, 659 (1986); M. Sano, S. Sato, and Y. Sawada, Prog. Theor. Phys. 76, 945 (1986); R. Badii and A. Politi, Phys. Rev. A 35, 1288 (1987); P. Szeplafalusy, T. Tel, A. Csordas, and Z. Kovacs, Phys. Rev. A 36, 3525 (1987).
24. J.L. Kaplan and J.A. Yorke, in Lecture Notes in Mathematics, vol. 730, eds. H.O. Peitgen and H.O. Walther (Springer, Berlin, 1979) p. 204; P. Frederickson, J.L. Kaplan, E. Yorke, and J. A. Yorke, J. Diff. Eqs. 49, 185 (1983).
25. I. Shimada and T. Nagashima, Prog. Theor. Phys. 61, 1605 (1979).
26. For example see: M. Dubois, Nucl. Phys. B (Proc. Suppl.) 2, 339 (1987).
27. S. Smale, Bull. Am. Math. Soc. 73, 747 (1967); S. Newhouse, D. Ruelle, and F. Takens, Commun. Math. Phys. 64, 35 (1978).
28. R. Stoop, J. Peinke, and J. Parisi, Phys. Rev. A (to be published).

Resumo

O comportamento não-linear do transporte de corrente durante o colapso de **germanio** intrínseco por **ionização** de impacto a baixas temperaturas engloba o desenvolvimento auto-sustentado de estruturas dissipativas tanto espacialmente filamentosas quanto temporalmente **oscilatorias** ao semiconductor inicialmente **homogêneo**. Estudamos os fenômenos de colapso **espaço-temporais cooperativos** por métodos de caracterização tanto probabilísticos como dinâmicos. O acordo entre os resultados obtidos a partir dos diferentes conceitos numéricos dá um quadro auto-consistente da **situação física** investigada. Em consequência, a hierarquia caótica obtida, de **atratores estranhos generalizados** do tipo ferradura, pode ser atribuída ao acoplamento não-linear fraco entre centros localizados de oscilação, intrínsecos do semi-condutor, e mutuamente competitivos.